Hindawi
Scientific Programming
Volume 2021, Article ID 8982101, 10 pages
https://doi.org/10.1155/2021/8982101

Research Article

Computed Tomography Images under Optimized Iterative Reconstruction Algorithm for Blood Flow Field Characteristics in Cerebral Aneurysm before and after Stent Implantation

Changkun Lin, Chuizhi Huang, Yan Chen, Nailong Jia, Jinghui Huang, and Qimao Fu

Department of Radiology, The Second Affiliated Hospital of Hainan Medical University, Haikou 570311, Hainan, China

Correspondence should be addressed to Qimao Fu; 201502210230@lzpcc.edu.cn

Received 18 May 2021; Revised 12 July 2021; Accepted 20 July 2021; Published 28 July 2021

Academic Editor: Gustavo Ramirez

In order to study the analysis of blood flow field characteristics of cerebral aneurysm patients before and after stent implantation based on CT images of ART-TV-PI, this paper firstly improved the ART-TV algorithm of algebraic reconstruction technology and obtained the ART-TV-PI algorithm, which was compared with the ART algorithm and ART-TV algorithm. Afterwards, the CT images based on the above three algorithms were used to analyze the changes of average blood flow velocity, average wall pressure, average wall deformation, and average shear force of 48 cases of cerebral aneurysm patients before and after stent implantation. The results showed that the mean square error and radiation dose of the ART-TV-PI algorithm (0.00012 and 1.65 mSv) were significantly lower than those of the ART algorithm (0.0031 and 3.09 mSv) and ART-TV algorithm (0.00082 and 2.52 mSv), and the signal-to-noise ratio (23.94) was significantly higher than those of the ART algorithm (11.32) and ART-TV algorithm (16.89), with statistically significant differences ($P < 0.05$). The differences of mean blood flow velocity, mean wall pressure, mean wall deformation, and mean shear force before and after stent implantation among the three algorithms were not statistically significant ($P > 0.05$), and the average index of the ART-TV-PI algorithm was the highest. Under the ART-TV-PI algorithm, the mean blood flow velocity (0.044 m/s), the mean wall pressure (71.7 Pa), the mean wall deformation (0.057 mm), and the mean shear force (889 Pa) after stent implantation were significantly lower than those before stent implantation (0.165 m/s, 160.8 Pa, 0.721 mm, and 2690 Pa), with average decreases of 73.3%, 55.4%, 92.1%, and 64.3%, respectively, and the differences were statistically significant ($P < 0.05$). In conclusion, the images reconstructed by the ART-TV-PI algorithm have good image quality, which provides great convenience for surgical examination of cerebral aneurysm stent implantation and is worthy of clinical application.

1. Introduction

In recent years, cardiovascular and cerebrovascular diseases have become the primary cause of threats to human health, with the changes in people's lifestyles and the aging of the population. By the end of 2013, there were approximately 230 million patients with cardiovascular and cerebrovascular diseases in China. However, this number has been still growing rapidly with the development of society [1]. Intracranial aneurysms account for the majority of all cardiovascular diseases. Intracranial aneurysms are the internal walls of cerebral arteries that bulge out locally due to pathological changes, forming a tumor-like protrusion. Besides, the cerebral aneurysm is the main cause of subarachnoid hemorrhage in patients, and its fatality rate and disability rate are extremely high, which seriously threatens people's health and quality of life [2, 3].

Cerebral aneurysm is highly latent, and the clinical symptoms usually appear late, but the damage is great after the onset of this disease [4]. Clinical studies have found that the predisposing factors of cerebral aneurysm are mainly genetic factors, atherosclerosis (AS), hypertension, vascular injury, traumatic infection, and so forth. [5]. At present, the treatment of cerebral aneurysms is divided into medical treatment and surgical treatment. Medical treatment is a traditional conservative treatment method, which is mostly

used for early remission of cerebral aneurysms or families with limited economic capacity. What is more, surgical treatment includes brain aneurysm tailoring or clipping, vascular interventional embolization of cerebral aneurysms, and cerebral vascular stent implantation [6, 7]. Moreover, cerebral vascular stent implantation has been a new research direction in recent years. Its principle can be simply explained as follows: the stent is compressed and implanted in a thin catheter. Then, the catheter follows the blood flow into the patient's cerebral aneurysm body, and the balloon is adopted to mechanically expand the blood vessel near the tumor. The catheter enters the stretched blood vessel segment, and the stent is inserted into the blood vessel. It can improve the eddy current imaging of the patient's blood flow field and reduce the blood deposition in the blood vessels of the tumor [8]. Endovascular interventional stent therapy is featured with low clinical trauma, low mortality, short surgical time, and less pain. However, it may lead to intravascular thrombosis in patients after stent implantation, which will cause vascular restenosis [9, 10]. Therefore, the above belongs to still difficult problems that need to be solved in the treatment of stent implantation.

With the rapid development of medical imaging technology, an excellent method is provided for the measurement of cerebral aneurysm. The investigation of the influence of the geometrical factors of cerebral aneurysm on the blood flow field is extremely critical, which undoubtedly depends on medical imaging detection [11]. The current detection method for cerebral aneurysms is mainly CT imaging. CT helps clinicians clearly observe the patient's tissue shape and lesion size and provides sufficient evidence for precise treatment. However, the collected images contain obvious noise, image artifacts, and distortion in actual detection due to irregular geometric shapes of cerebral aneurysm blood vessels and pulsation of blood [12, 13], which brings a lot of troubles to the diagnosis of clinicians. In addition, the CT imaging method is to scan the patient with X-rays, which will cause the patient to be exposed to ionizing radiation at the same time. High-dose radiation may damage the patient's immune system and blood system to increase the risk of leukemia and cancer, thereby resulting in irreversible damage to the patient's body [14]. Lv and Xiu [15] added the nonlocal idea to the total variation model, proposed a nonlocal total variation model, and established an energy functional model for the noisy images, which tended to be minimized by iterative solution, thus greatly improving the level of image denoising. In order to deal with multiple artifacts, noise, and strong radiation in CT imaging, ART-TV was optimized in this study to obtain a new algorithm ART-TV-PI. Then, ART-TV-PI was applied in the analysis of blood flow field characteristics before and after implantation of aneurysm stents. This study aimed to provide a theoretical basis for CT imaging examination of cerebral vascular stent implantation for the treatment of cerebral aneurysms.

2. Materials and Methods

2.1. Research Objects. In this study, 48 patients with cerebral aneurysms were selected as the research objects, who were treated at the hospital from June 2017 to June 2019. Besides, each patient received a CT examination. Among the 48 patients, 16 were male and 32 were female. They were 40–64 years old, with an average age of 55 ± 6.32 years. CT images based on ART algorithm, ART-TV algorithm, and ART-TV-PI algorithm were used to analyze the blood flow field characteristics of each patient with cerebral aneurysm before and after stent implantation. This study had been approved by the Medical Ethics Committee of the hospital, and the patients and their family members had known this study and signed the informed consent forms.

Inclusion criteria: (1) patients in line with age; (2) patients with complete clinical and imaging data; and (3) patients undergoing stent implantation.

Exclusion criteria: (1) patients who have undergone other brain operations before; (2) patients who cannot undergo cranial CT examination due to pacemaker and claustrophobia; (3) patients with unclear CT images; and (4) patients who failed to cooperate with signing an informed consent form.

2.2. CT Scanning Parameter Setting. In this study, a dual-source CT machine (SIEMENS SOMATOM Definition Flash) was used for scanning. The spiral scanning parameters were as follows. The collimation width was 0.625 mm, screw pitch was 0.961 mm, and iDose was used for reconstruction. The distance of the X-ray source to the center of rotation was set as 380 mm, and the distance of the S-ray source to the detector was 760 mm. The number of detector elements on the detector was 480, the initial scanning position was y-axis, the scanning degree of ray source rotating counterclockwise was 120°, and the number of iterations was set to 120 times to ensure the smooth convergence of CT images. The scanning data were collected through the maximum intensity projection (MIP) and volume reconstruction (VR) methods. What is more, contrast agents were injected for patients with different conditions. Ulrich high-pressure syringes and BDSaf-T-Intima 20GA injection needles were applied in this study, iohexol was selected as a contrast agent, with a concentration of 340 g/L. A high-pressure bolus injection was used, and the total dose was 45–85 mL. Moreover, the average injection rate was 4.8 mL/s, and the injection site of the contrast agent was the middle cubital vein. After the injection, normal saline was employed to rinse. The resolution of the CT scanning images in this study was 512×512, and the scanning data were stored.

2.3. Implementation of Iterative Reconstruction Algorithm after Optimization. Iterative reconstruction algorithms have great advantages for CT limited-angle scanning, and iterative algorithms include ART and simultaneous ART (SART). ART usually acts on the discrete-discrete model, and its basic idea is to initially assign the reconstructed CT image, and then, the projection data of the image are obtained according to the orthographic projection Besides, the estimated data are compared with the projection data, and the image is updated through the back projection of correction results. Therefore, the reconstructed images that meet the conditions are iteratively obtained in this way [15], as shown in Figure 1.

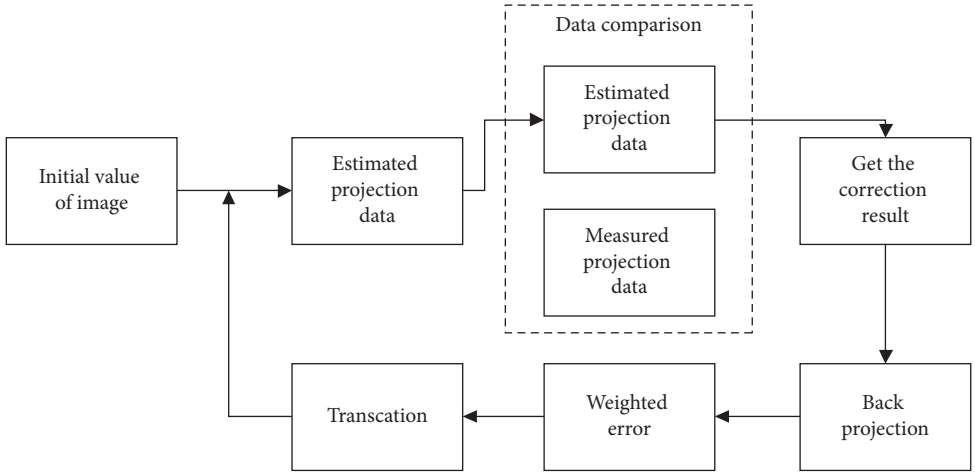

Figure 1: ART algorithm solving process.

When the image was processed, it was assumed that the initial value of the initial image at any projection angle was f_i and the ray at this projection angle was set as l. Thus, the projection of the image at this angle could be expressed as follows:

$$\rho_l' = \sum_{i=1}^{N} w_{li} f_i, \tag{1}$$

where ρ_l' represents the estimated projection under the angle, w_{li} stands for the weight of the i-th grid to the l-th ray, and N means the number of grids. Then, the error between the actual projection data and the estimated projection data is shown in the following:

$$\Delta_l = \rho_l - \rho_l', \tag{2}$$

where Δ_l represents the projection error and ρ_l stands for the actual projection data. By using the error to calculate the correction value of the pixel point that passed through the l-th ray, it can be expressed by the following equation:

$$P_i = \Delta_l \frac{w_{li}}{\sum_{i=1}^{N} w_{li}^2}, \tag{3}$$

where P_i stands for the pixel correction value. According to equation (3), the pixel correction value of all rays under the projection angle was calculated, which was regarded as a complete iteration. Then, whether the termination condition was met should be determined. If not, the previous iteration result was used as the initial value of the image to continue repeating the above operation. The iterative equation of the ART algorithm could be expressed by the following function:

$$f_i^{n+1} = f_i^n + \lambda \frac{w_{li}}{\sum_{i=1}^{N} w_{li}^2} \left(\rho_l - \sum_{i=1}^{N} w_{li} f_i^n \right), \tag{4}$$

where$n$ expresses the number of iterations of the ART algorithm and λ means the relaxation factor. The ART algorithm could be adopted in different data collection modes and can reconstruct images for some situations such as insufficient projection angle, uneven angle, and missing projection data. However, the ART algorithm had a large amount of calculation and slow calculation speed, which occupied a lot of memory. When applying sparse angle projection data, the reconstruction results of the ART algorithm often could not meet the requirements [16]. Therefore, it was necessary to add constraints to the ART algorithm for reconstruction.

A TV model was introduced in the objective function of the ART algorithm as an algorithm constraint. For an image of size $H \times H$, its TV could be represented by the following function:

$$\begin{aligned} \mathrm{TV}(m) &= \|\nabla m\|_1 \\ &= \sum_{l,i} |\nabla_{l,i}|, \end{aligned} \tag{5}$$

where $|\nabla_{l,i}|$ can be calculated as follows:

$$|\nabla_{l,i}| = \sqrt{\left(m_{l,i} - m_{l-1,i}\right)^2 + \left(m_{l,i} - m_{l,i-1}\right)^2 + z}, \tag{6}$$

where z represents a small positive real number, and its role is to prevent the TV algorithm from appearing when the denominator is 0 during the derivation process. By introducing the TV algorithm into the ART algorithm, the reconstructed ART-TV algorithm model was obtained, as shown in the following function:

$$\begin{aligned} &\min \|m\|_{\mathrm{TV}} \\ &\text{s.t.} \quad Am = \rho, \end{aligned} \tag{7}$$

where A means the system matrix. Based on the function expression of the ART-TV algorithm, the solution process of the ART-TV algorithm could be gotten. Firstly, there was a setting for the initial value and algorithm related parameters of the initialization image. Then, the estimated projection data and the actual projection data of the initialized image at any angle were obtained to carry out the reconstruction of the ART algorithm. After the image was reconstructed, there was a nonnegative correction operation to correct all pixels with a pixel value less than 0 under the projection angle to 0. Finally, the gradient descent method was employed to

minimize the reconstructed image. If the termination condition was not satisfied, the above steps should be repeated [17].

In clinical CT scanning, patients undergoing CT scanning receive larger radiation doses due to the large scanning range and long scanning time. The second scanning often results in the difference between the patient's anatomical structure information and the prior image information because of the movement of the patient's organs and positioning errors [18]. Clinical studies have found that bones, muscles, and other relatively uniform substances contained in CT scanning images can extract their average pixel values as the prior values of CT scanning to construct CT images [19]. Therefore, this image construction algorithm has been called the ART-TV-PI algorithm, and the algorithm model can be represented by the following function:

$$\begin{aligned} &\min \|m\|_{\mathrm{TV}} + \lambda * f(m, PI) \\ &\text{s.t. } Am = \rho, \end{aligned} \tag{8}$$

where λ and PI stand for the weighting factor and the prior value of CT scanning in turn. By transforming equation (8), the following function can be obtained:

$$\begin{aligned} &\min \sum_{l,i} \sqrt{\left(m_{l,i} - m_{l-1,i}\right)^2 + \left(m_{l,i} - m_{l,i-1}\right)^2 + z} + \lambda * \sum_{l,i} \sqrt{\left(m_{l,i} - PI_{l,i}\right)^2 + z} \\ &\text{s.t. } Am = \rho. \end{aligned} \tag{9}$$

Through equations (8) and (9), the solution process of the ART-TV-PI algorithm could be obtained as follows: first, the high-quality image similar to the image to be reconstructed from the patient's previous scanning was taken as the prior image, thereby calculating the average pixel value of uniform substance in the image to be the prior value. Then, there were the initial value and algorithm related parameter settings for the image. The ART algorithm was reconstructed by applying the estimated projection data and the actual projection data. After the image was reconstructed, the image was subjected to a nonnegative correction operation, and all pixels with a pixel value less than 0 were corrected to 0 under the projection angle. Last, the reconstructed image was minimized by the gradient descent method. If the termination condition was not met, the above steps were continued to be repeated.

2.4. Evaluation Standards of Image Quality. The most intuitive evaluation method for CT image quality is visual judgment, but this subjective judgment method will produce different judgment results due to personal experience. Thus, MSE and SNR were introduced in this study to comprehensively judge the image quality. MSE is the average error between the ideal image and the reconstructed image based on different algorithms. The smaller the MSE, the smaller the error of the reconstructed image. Moreover, the SNR value reflects the noise level of the reconstructed image based on different algorithms. The larger the SNR, the smaller the noise of the reconstructed image. The calculation method of MSE and SNR could be expressed by the following functions:

$$\mathrm{MSE} = \frac{1}{S} \sum_{i}^{S} \left(g_i' - g_i\right)^2, \tag{10}$$

$$\mathrm{SNR} = 10 \log_{10} \left(\frac{\sum_i^S \left(g_i - \overline{g_i}\right)^2}{\sum_i^S \left(g_i' - g_i\right)^2} \right). \tag{11}$$

In equations (10) and (11), S means the number of pixels on the reconstructed image and g_i', g_i, and $\overline{g_i}$ stand for the pixel gray value of the ideal image, the pixel gray value of the reconstructed image, and the pixel average value of the reconstructed image, respectively.

2.5. Evaluation Standard of Radiation Dose. When different iterative reconstruction algorithms were applied to scan the cerebral aneurysm of each patient, the volume CT dose index (CTDI) and dose length product (DLP) values of each scanning were recorded, and the effective radiation dose (ED) of each scanning was calculated after the scanning was over. In addition, the value of ED was the product of DLP and the conversion factor, and the conversion factor in this study was 0.014 mSv/(mGy.cm).

2.6. Evaluation Standards of Blood Flow Field Characteristics. The blood flow in the cerebral aneurysm was considered as a long flow, which meant that the movement factor at a certain point in the blood flow field did not change with time. Therefore, all fluids in the blood flow field should satisfy the continuity equation and the law of conservation of mass. The continuity equation of blood flow in the blood flow field could be derived, as shown in the following:

$$\frac{\partial(\rho v_x)}{\partial x} + \frac{\partial(\rho v_y)}{\partial y} + \frac{\partial(\rho v_z)}{\partial z} = 0, \tag{12}$$

where ρ represents the fluid density of the blood flow field; v expresses the average velocity of the blood flow field fluid; and v_x, v_y, and v_z stand for the three components of the fluid velocity in the directions of x, y, and z in sequence. Besides, the momentum equations in the three directions (x, y, and z) could be derived according to Newton's second law:

$$\frac{\partial v_x}{\partial t} + v_x\frac{\partial v_x}{\partial x} + v_y\frac{\partial v_x}{\partial y} + v_z\frac{\partial v_x}{\partial z} = -\frac{1\partial P}{\rho\partial x} + Gx + n\nabla^2 v_x, \quad (13)$$

$$\frac{\partial v_y}{\partial t} + v_x\frac{\partial v_y}{\partial x} + v_y\frac{\partial v_y}{\partial y} + v_z\frac{\partial v_y}{\partial z} = -\frac{1\partial P}{\rho\partial y} + Gy + n\nabla^2 v_y, \quad (14)$$

$$\frac{\partial v_z}{\partial t} + v_x\frac{\partial v_z}{\partial x} + v_y\frac{\partial v_z}{\partial y} + v_z\frac{\partial v_z}{\partial z} = -\frac{1\partial P}{\rho\partial z} + Gz + n\nabla^2 v_z. \quad (15)$$

In equations (13)–(15), t stands for the time, P expresses the fluid pressure, G indicates the unit mass force in different directions, n represents the dynamic viscosity, $-(1\ \partial P/\rho\ \partial z)$ means the pressure exerted on the fluid, Gz stands for the fluid volume force, and $n\nabla^2 v_z$ expresses the wall shear force. What is more, the four indexes of flow velocity, pressure, volume force, and wall shear force were analyzed, so as to determine the characteristics of the blood flow field in the cerebral aneurysm before and after the stent implantation.

2.7. Statistical Analysis. SPSS 17.0 statistical software was adopted to process the data of this study. CT value, radiation dose, MSE, SNR, blood flow velocity, wall pressure, wall deformation, wall shear force, and other measurement data were expressed as $\overline{x}$, and the t-test was used for data between groups. Besides, the order and test of multisample comparison were applied in the reconstruction image quality evaluation. The count data were represented by n (%), which was detected by χ^2 test, and the q test was used for the pairwise comparison. In addition, $P < 0.05$ meant that the difference was statistically substantial.

3. Experimental Results

3.1. Analysis of CT Scanning Results Based on Different Iterative Algorithms. The CT scanning parameters in Section 2.2 were applied to analyze the brain before and after stent implantation in each patient with cerebral aneurysm, and the scanning results are shown in Figures 2–4. They showed clearly that there were still a lot of noises in the ART scanning group after 120 iterations, and the ART-TV scanning group had obvious artifacts. Besides, there was a certain degree of edge loss in the ART scanning group and the ART-TV scanning group. The scanning effect of the ART-TV-PI scanning group proposed in this study was good compared with the ART scanning group and the ART-TV scanning group. The CT scanning images of the ART-TV-PI scanning group showed complete edge structure information, clear image contours, and no obvious artifacts before and after the stent implantation. In this study, the surgical method was LVIS stent implantation. The preoperative angiography presented an obvious saccular expansion of the arterial segment. After the surgery, the cerebral aneurysm was not imaged again, the metastatic artery was well developed, and the blood supply of each branch of the artery was good. Furthermore, the results are shown in Figure 5. There are many more images of capillaries after implantation than before.

3.2. Analysis of MSE and SNR Based on Different Iterative Reconstruction Algorithms. MSE and SNR indexes were adopted to analyze the image quality of the reconstructed CT images before and after the stent implantation. The number of iterations was set to 120, thereby ensuring the smooth convergence of the images. After scanning, the values of MSE and SNR were calculated based on different iterative algorithms, as shown in Figures 6 and 7. The results showed that the MSE and SNR of the ART scanning group were 0.0031 and 11.32 in turn after 120 iterations, and the values of the ART-TV scanning group were 0.00082 and 16.89, respectively. In addition, those of the ART-TV-PI scanning group after 120 iterations were 0.00012 and 23.94, respectively. The difference between any two groups was statistically marked ($P < 0.05$). Among the three algorithms, the ART-TV-PI algorithm applied in this study has a smaller MSE and a higher SNR compared with the ART algorithm and the ART-TV algorithm, which indicated that the image quality reconstructed by the ART-TV-PI algorithm was better and the reconstructed image was closer to the real image.

3.3. Analysis of Radiation Dose Based on Different Iterative Reconstruction Algorithms. After the CT scanning of patients in different iterative algorithm groups was completed, the ED value of each scanning was calculated for comparison and analysis (Figure 8). The results showed that the average CTDI, DLP, and ED values of the ART scanning group were 15.35 mGy, 220.42 mGm.cm, and 3.09 mSv, respectively; the average CTDI, DLP, and ED values of the ART-TV scanning group were 11.41 mGy, 179.88 mGm.cm, and 2.52 mSv in turn; the average CTDI, DLP, and ED values of the ART-TV-PI scanning group were 7.63 mGy, 118.15 mGm.cm, and 1.65 mSv, respectively. The difference between the results of the three groups is statistically significant ($P < 0.05$).

3.4. Analysis of Blood Flow Field Characteristics before and after Stent Implantation Based on CT Images of Different Algorithms. Figure 9 is a graph showing the changes in the average blood flow velocity before and after stent implantation based on CT image analysis of different algorithms. As can be seen from the graph, the average blood flow velocity before and after stent implantation under the ART algorithm is 0.155 m/s and 0.038 m/s, respectively, and the average blood flow velocity before and after stent implantation under the ART-TV algorithm is 0.162 m/s and 0.041 m/s, respectively. The mean blood flow velocities before and after stent implantation using ART-TV-PI algorithms were 0.165 m/s and 0.044 m/s, respectively. No matter the mean blood flow velocities before stent implantation or after stent implantation using the three algorithms, the differences between them were not statistically significant ($P > 0.05$). Under the ART-TV-PI algorithm, the average blood flow velocity after stent implantation is significantly lower than that before stent implantation, with an average decrease of 73.3%, and the difference is statistically significant ($P < 0.05$).

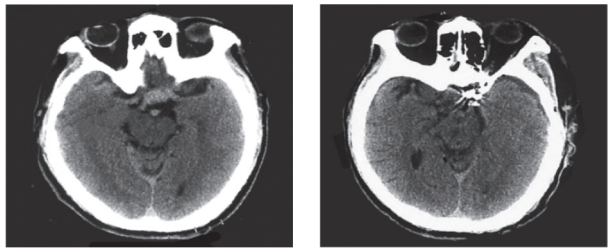

(a) (b)

Figure 2: The scanning results of the ART scanning group before and after stent implantation. (a) Postoperative. (b) Preoperative.

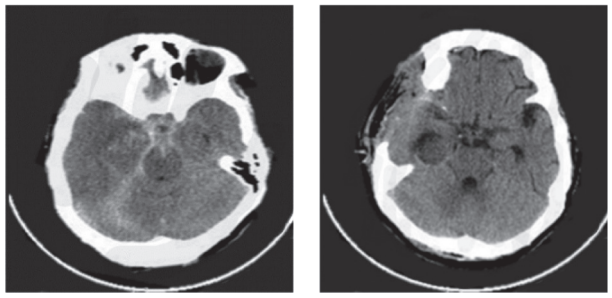

(a) (b)

Figure 3: The scanning results of the ART-TV scanning group before and after stent implantation. (a) Postoperative. (b) Preoperative.

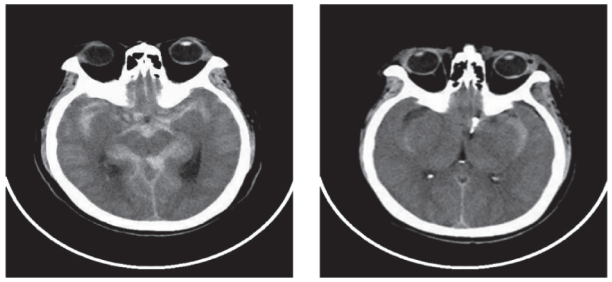

(a) (b)

Figure 4: Scanning results of the ART-TV-PI scanning group before and after stent implantation. (a) Postoperative. (b) Preoperative.

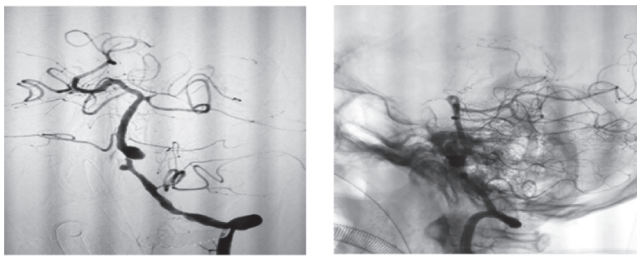

(a) (b)

Figure 5: The results of surgical imaging before and after stent implantation. (a) Postoperative. (b) Preoperative.

Figure 10 is a graph showing the changes in the average wall pressure before and after stent implantation based on CT image analysis of different algorithms. As can be seen from the graph, the average wall pressure before and after stent implantation under the ART algorithm is 152.7 Pa and 64.2 Pa, respectively, and the average wall pressure before

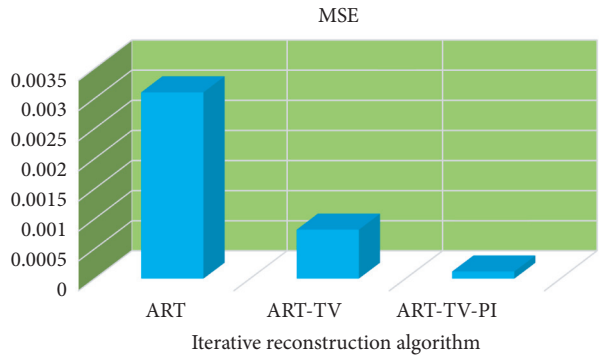

Figure 6: Comparison of MSE based on different iterative reconstruction algorithms.

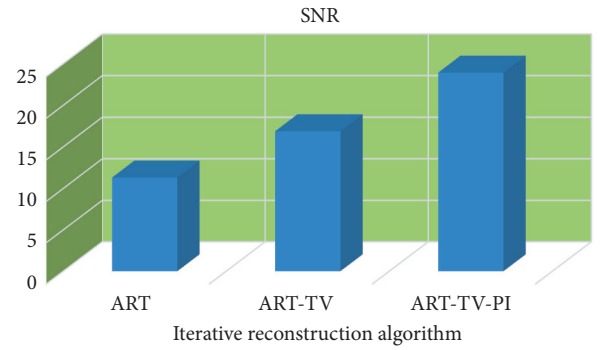

Figure 7: Comparison of SNR based on different iterative reconstruction algorithms.

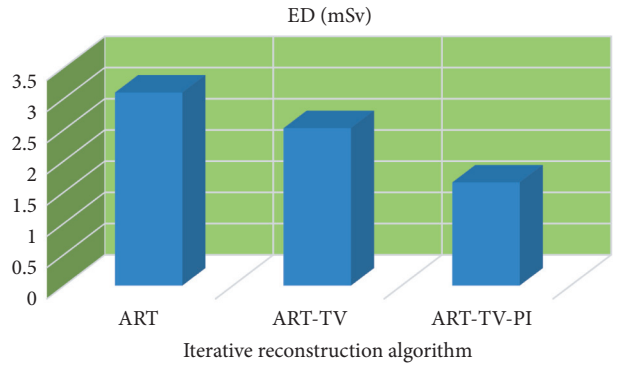

Figure 8: Comparison of ED values based on different iterative algorithms.

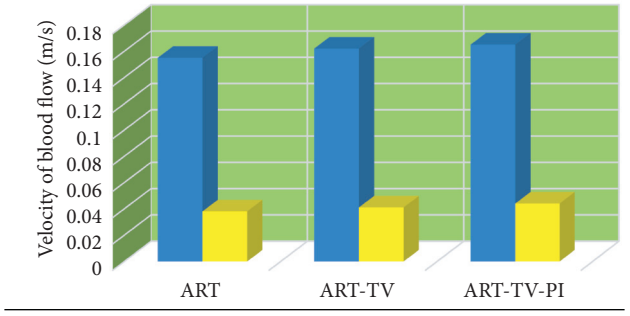

Preoperative	0.155	0.162	0.165
Postoperative	0.038	0.041	0.044

Figure 9: CT images based on different algorithms to analyze the changes of mean blood flow velocity before and after stent implantation.

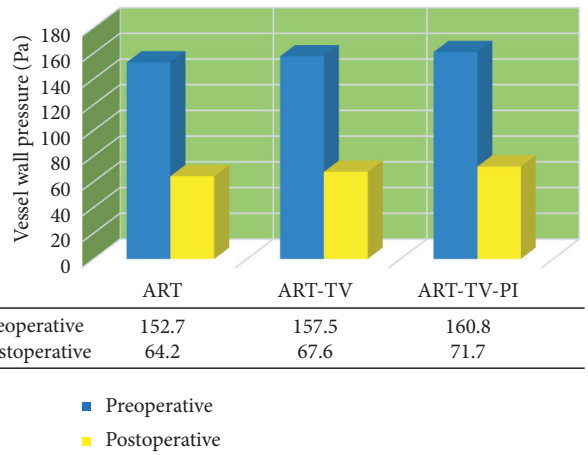

Figure 10: CT images based on different algorithms to analyze the changes of mean wall pressure before and after stent implantation.

and after stent implantation under the ART-TV algorithm is 157.5 Pa and 67.6 Pa, respectively. The mean wall pressures before and after stent implantation using ART-TV-PI algorithms were 160.8 Pa and 71.7 Pa, respectively. No matter the mean wall pressures before stent implantation or after stent implantation using the three algorithms, the differences between them were not statistically significant ($P > 0.05$). Under the ART-TV-PI algorithm, the average wall pressure after stent implantation is significantly lower than that before stent implantation, with an average reduction of 55.4%, and the difference is statistically significant ($P < 0.05$).

Figure 11 is a graph showing the changes in the average wall deformation before and after stent implantation based on CT image analysis of different algorithms. As can be seen from the graph, the average wall deformation before and after stent implantation under the ART algorithm is 0.694 mm and 0.042 mm, respectively, and the average wall deformation before and after stent implantation under the ART-TV algorithm is 0.718 mm and 0.053 mm, respectively. The average wall deformations before and after stent implantation using ART-TV-PI algorithms were 0.721 mm and 0.057 mm, respectively. No matter the average wall deformations before stent implantation or after stent implantation using the three algorithms, the differences between them were not statistically significant ($P > 0.05$). Besides, the average wall deformation after stent implantation using the ART-TV-PI algorithm was significantly lower than that before stent implantation, with an average reduction of 92.1%, and the difference was statistically significant ($P < 0.05$).

Figure 12 is a graph showing the changes in the average shearing force before and after stent implantation based on CT image analysis of different algorithms. As can be seen from the graph, the average shearing force before and after stent implantation under the ART algorithm is 2523 Pa and 826 Pa, respectively, and that before and after stent implantation under the ART-TV algorithm is 2590 Pa and 839 Pa, respectively. The average shear forces before and after stent implantation under the ART-TV-PI algorithm were 2690 Pa and 889 Pa, respectively. No matter the average shear forces before stent implantation or after stent implantation under the three algorithms, the differences between them were not statistically significant ($P > 0.05$). Under the ART-TV-PI algorithm, the average shearing force after stent implantation is significantly lower than that before stent implantation, the average shearing force is reduced by 64.3%, and the difference is statistically significant ($P < 0.05$).

4. Discussion

Cerebral aneurysm is currently one of the major diseases threatening human health [16]. In the surgical treatment of cerebral aneurysms, stent implantation is a hot research topic [17]. In order to obtain high-quality CT images for clinical application of stent implantation in the treatment of cerebral aneurysms, in this study, the ART-TV algorithm was improved firstly, and a new iterative reconstruction algorithm, ART-TV-PI, was obtained and compared with the ART algorithm and ART-TV algorithm. The results showed that the SNR of the ART-TV-PI algorithm (23.94) was significantly higher than that of the ART algorithm (11.32) and ART-TV algorithm (16.89), and the difference was statistically significant ($P < 0.05$). The mean square error (0.00012) and radiation dose (1.65 mSv) of the ART-TV-PI algorithm are significantly lower than those of the ART algorithm (0.0031, 3.09 mSv) and ART-TV algorithm (0.00082, 2.52 mSv), and the difference is statistically significant ($P < 0.05$), suggesting that the image quality reconstructed by the ART-TV-PI algorithm is better, closer to the real image, and it causes less damage to the patient during the CT scan. This result is similar to that of Zhang and Liu [18], and after the ART algorithm is optimized, all performance indexes are superior to those before improvement.

Then, the CT images based on the above three algorithms were used to analyze the blood flow field characteristics of 48 patients with cerebral aneurysm before and after stent implantation. The results showed that the differences were not statistically significant ($P > 0.05$) for the mean blood flow velocity, the mean wall pressure, the mean wall deformation,

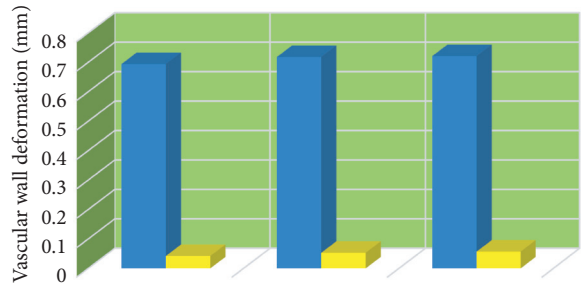

	ART	ART-TV	ART-TV-PI
Preoperative	0.694	0.718	0.721
Postoperative	0.042	0.053	0.057

Figure 11: CT images based on different algorithms to analyze the changes of average wall deformation before and after stent implantation.

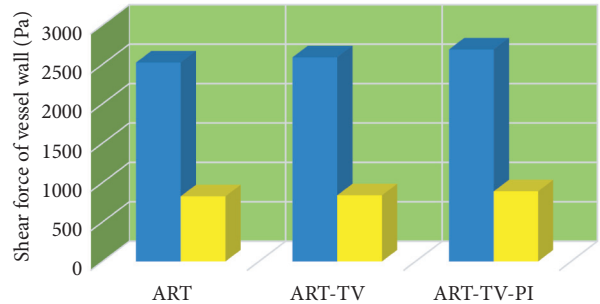

	ART	ART-TV	ART-TV-PI
Preoperative	2523	2590	2690
Postoperative	826	839	889

Figure 12: CT images based on different algorithms to analyze the changes of average shear force before and after stent implantation.

the mean shear force, and those after stent implantation under the three algorithms, and the average index under ART-TV-PI algorithm was the highest. Under the ART-TV-PI algorithm, the average blood flow velocity (0.044 m/s) after stent implantation is significantly lower than that before stent implantation (0.165 m/s), with a mean reduction of 73.3%, and the difference is statistically significant ($P < 0.05$). Under the ART-TV-PI algorithm, the average wall pressure after stent implantation (71.7 Pa) was significantly lower than that before stent implantation (160.8 Pa), and the average reduction was 55.4%, with a statistically significant difference ($P < 0.05$). Under the ART-TV-PI algorithm, the average wall deformation after stent implantation (0.057 mm) is significantly lower than that before implantation (0.721 mm), and the average reduction is 92.1%, with a statistically significant difference ($P < 0.05$). Under the ART-TV-PI algorithm, the average shear force (889 Pa) after stent implantation is significantly lower than that before stent implantation (2690 Pa), the average reduction is 64.3%, and the difference is statistically significant ($P < 0.05$). This result was consistent with that of Yuan et al. [19]. After the stent implantation, the average blood flow velocity, the average wall pressure, the average wall deformation, and the average shear force of the patients were greatly improved. These results indicate that the characteristic parameters of the blood flow field of patients have significant changes after stent implantation, and the therapeutic effect of stent implantation on cerebral aneurysm is significant.

5. Conclusion

In this study, the quality of reconstructed CT images of cerebral aneurysms obtained by ART algorithm, ART-TV algorithm, and ART-TV-PI iterative reconstruction algorithm before and after stent implantation was evaluated, and the blood flow field characteristics before and after stent implantation were analyzed. The results revealed that the ART-TV-PI algorithm had a marked effect on removing noise and artifacts from CT images, and the reconstructed images were featured with excellent quality and low radiation dose. After stent implantation, the patient's blood flow field characteristics were changed dramatically, so stent

implantation had a good application prospect for the treatment of cerebral aneurysms. However, there are few cases in this study and no long-term follow-up analysis of the patient's body indexes after stent implantation. Therefore, it will be further improved in future work.

Data Availability

The data used to support the findings of this study are available from the corresponding author upon request.

Conflicts of Interest

The authors declare no conflicts of interest.

Authors' Contributions

Changkun Lin and Chuizhi Huang contributed equally to this work.

References

[1] G. D. Liu, H. Wang, Q. Wang et al., "The prevalence and coping strategies for four main chronic non-communicable diseases," *Chinese Journal of Social Medicine*, vol. 34, no. 1, pp. 53–56, 2017.

[2] N. Etminan and G. J. E. Rinkel, "Cerebral aneurysm guidelines-more guidance needed," *Nature Reviews Neurology*, vol. 11, no. 9, pp. 490-491, 2015.

[3] A. E. Hussein, D. Brunozzi, S. F. Shakur, R. Ismail, F. T. Charbel, and A. Alaraj, "Cerebral aneurysm size and distal intracranial hemodynamics: an assessment of flow and pulsatility index using quantitative magnetic resonance angiography," *Neurosurgery*, vol. 83, no. 4, pp. 660–665, 2018.

[4] Y. G. Liao, "Study on the treatment strategy and risk factor intervention of cerebral aneurysm," *Journal of Diseases Monitor & Control*, vol. 10, no. 8, pp. 622–624, 2016.

[5] R. L. Shen, J. S. Qi, Y. D. Zhang et al., "Clinical analysis of the risk factors of cerebral artery aneurysm," *Journal of Henan University of Science & Technology, (Medical Science)*, vol. 68, no. 4, pp. 262–264, 2015.

[6] T. Konno, T. Mashiko, H. Oguma et al., "Rapid 3-dimensional models of cerebral aneurysm for emergency surgical clipping," *Noshinkeigeka*, vol. 44, no. 8, pp. 651–660, 2016.

[7] Q. L. Xu and L. Yan, "Clinical effects of microsurgical clipping and vascular embolization on patients with cerebral aneurysms," *Chinese Journal of Preventive Medicine*, vol. 45, no. 4, pp. 15–18, 2018.

[8] X. Y. Liu, K. Muhetaer, G. Ju et al., "Blood flow field characteristics of cerebral aneurysm before stent implantation," *Chinese Journal of Tissue Engineering Research*, vol. 20, no. 38, pp. 5722–5729, 2016.

[9] J. F. Zhong, B. Li, T. K. Tang et al., "The clinical effects and complications of intravascular stent in the treatment of intracranial wide-necked aneurysms," *E-Journal of Translational Medicine*, vol. 3, no. 4, pp. 21-22, 2016.

[10] C. L. Hu, K. Muhetaer, G. W. Zhang et al., "Numerical simulation of hemodynamic effects of endovascular stent on the area of intracranial aneurysms," *Journal of Biomedical Engineering Research*, vol. 35, no. 4, pp. 241–244, 2016.

[11] M. Dabagh, P. Nair, J. Gounley, D. Frakes, L. F. Gonzalez, and A. Randles, "Hemodynamic and morphological characteristics of a growing cerebral aneurysm," *Neurosurgical Focus*, vol. 47, no. 1, p. E13, 2019.

[12] X. D. Lu, Y. Tian, and B. Li, "Analysis of CT diagnosis of ruptured cerebral aneurysm," *Medical Information*, vol. 29, no. 10, pp. 247-248, 2016.

[13] V. Dunet, M. Bernasconi, S. D. Hajdu, R. A. Meuli, R. T. Daniel, and J.-B. Zerlauth, "Impact of metal artifact reduction software on image quality of gemstone spectral imaging dual-energy cerebral CT angiography after intracranial aneurysm clipping," *Neuroradiology*, vol. 59, no. 9, pp. 845–852, 2017.

[14] D. Q. Wang and Y. L. Liu, "Multislice spiral CT examination control of radiation hazards," *Chinese Journal of Radiological Health*, vol. 25, no. 5, pp. 569–572, 2016.

[15] Z. Lv and W. Xiu, "Interaction of edge-cloud computing based on SDN and NFV for next generation IoT," *IEEE Internet of Things Journal*, vol. 7, no. 7, pp. 5706–5712, 2019 Oct.

[16] H. Qi, Z. Chen, S. Wu, Y. Xu, and L. Zhou, "Iterative image reconstruction using modified non-local means filtering for limited-angle computed tomography," *Physica Medica*, vol. 32, no. 9, pp. 1041–1051, 2016.

[17] L. D. Mo and B. Q. Xu, "An improved TV image reconstruction algorithm," *Electronic Science and Technology*, vol. 29, no. 10, pp. 47–50, 2016.

[18] W. Y. Zhang and X. Y. Liu, "Application of three-dimensional reconstruction based on biomedical images," *Journal of Chinese Practical Diagnosis and Therapy*, vol. 30, no. 7, pp. 629–631, 2016.

[19] Y. Yuan, H. L. Qi, Q. S. Geng et al., "Prior image constrained total variation regularization CT image reconstruction algorithm," *Computer Engineering and Design*, no. 4, pp. 999–1003, 2015.